JOURNAL OF NEUROTRAUMA 29:1455–1468 (May 1, 2012)

DOI: 10.1089/neu.2011.2207

Use-Dependent Dendritic Regrowth Is Limited after Unilateral Controlled Cortical Impact to the Forelimb Sensorimotor Cortex

Theresa A. Jones,[1,*] Daniel J. Liput,[2,*] Erin L. Maresh,[1,*] Nicole Donlan,[1] Toral J. Parikh,[1] Dana Marlowe,[2] and Dorothy A. Kozlowski[2]

Abstract

Compensatory neural plasticity occurs in both hemispheres following unilateral cortical damage incurred by seizures, stroke, and focal lesions. Plasticity is thought to play a role in recovery of function, and is important for the utility of rehabilitation strategies. Such effects have not been well described in models of traumatic brain injury (TBI). We examined changes in immunoreactivity for neural structural and plasticity-relevant proteins in the area surrounding a controlled cortical impact (CCI) to the forelimb sensorimotor cortex (FL-SMC), and in the contralateral homotopic cortex over time (3–28 days). CCI resulted in considerable motor deficits in the forelimb contralateral to injury, and increased reliance on the ipsilateral forelimb. The density of dendritic processes, visualized with immunostaining for microtubule-associated protein-2 (MAP-2), were bilaterally decreased at all time points. Synaptophysin (SYN) immunoreactivity increased transiently in the injured hemisphere, but this reflected an atypical labeling pattern, and it was unchanged in the contralateral hemisphere compared to uninjured controls. The lack of compensatory neuronal structural plasticity in the contralateral homotopic cortex, despite behavioral asymmetries, is in contrast to previous findings in stroke models. In the cortex surrounding the injury (but not the contralateral cortex), decreases in dendrites were accompanied by neurodegeneration, as indicated by Fluoro-Jade B (FJB) staining, and increased expression of the growth-inhibitory protein Nogo-A. These studies indicate that, following unilateral CCI, the cortex undergoes neuronal structural degradation in both hemispheres out to 28 days post-injury, which may be indicative of compromised compensatory plasticity. This is likely to be an important consideration in designing therapeutic strategies aimed at enhancing plasticity following TBI.

Key words: dendritic arborization; forelimb deficits; forelimb sensorimotor cortex; synaptic density; traumatic brain injury

Introduction

Neural plasticity has been demonstrated after insults to both the peripheral and central nervous systems. This plasticity can occur from the molecular to the systems level in humans and other animals. In early work on neocortex, this was demonstrated to occur following peripheral nerve injury. Somatosensory cortex was shown to reorganize itself in monkeys following sensory deprivation produced by peripheral nerve injury (Kaas et al., 1983). The sensorimotor cortex has also been shown to exhibit plasticity following focal electrolytic lesions to the forelimb sensorimotor cortex (FL-SMC; Schallert et al., 1997), and following ischemic infarcts (Allred and Jones, 2008; Nudo, 2007).

We have previously found time-dependent increases in dendritic arborization of layer V pyramidal neurons in the cortex contralateral and homotopic to unilateral electrolytic or ischemic lesions of the FL-SMC. Arborization was found to be maximal at 18 days after electrolytic lesions, followed by pruning of the dendritic arbors to just above sham levels by day 30 (Jones and Schallert, 1992). Also seen at 30 days, but not at 10 or 18 days, were increases in synapse number per neuron in cortical layer V (Jones et al., 1996). Similarly, after an ischemic injury to the FL-SMC, significant increases in microtubule-associated protein (MAP-2) immunoreactive dendrites were seen in layer V of the contralateral homotopic cortex. These increases in MAP-2 were observed as early as day 2 post-injury and were maximal 14 days after injury

[1]University of Texas at Austin, Department of Psychology and Institute for Neuroscience, Austin, Texas.
[2]DePaul University, Department of Biological Sciences, Chicago, Illinois.
*These authors contributed equally to this article.

(Adkins et al., 2004). There were also increases in synapse numbers evident as early as 30 days after the lesions (Jones et al., 1996; Luke et al., 2004). Increases in Fos and NMDAR1 immunoreactivity were also seen in layers II/III and V. NMDAR1 immunoreactivity was significantly greater compared to sham animals at 14 days, while Fos was elevated only in layers II/III at 2 days (Adkins et al., 2004).

The above-mentioned dendritic growth and synaptogenesis were shown to be dependent on behavioral compensation following injury. After a unilateral electrolytic or stroke-like injury to the FL-SMC, the animal heavily relies on the unimpaired forelimb ipsilateral to the injury. When this forelimb is restrained beginning early following electrolytic lesions, the dendritic growth does not occur (Jones and Schallert, 1994; Kozlowski et al., 1996). However, cortical neuroplasticity is enhanced by motor rehabilitative training, such as reach training and acrobatic training (Hsu and Jones, 2005,2006; Luke et al., 2004). These findings add support for the idea that cortical neural plasticity is a mechanism underlying both behavioral compensation and rehabilitation efficacy (Jones et al., 2009).

Neocortical plasticity has been assumed to play a role in recovery of function following traumatic brain injury (TBI) as well (Lehr, 2010; Stein, 2007), but there is little evidence of such plasticity in the neocortex after this type of injury. In studies of the hippocampus, measures of gene expression, dendritic structure, and long-term potentiation (LTP) indicate that reactive neural plasticity can be remarkably limited after TBI (Ansari et al., 2008a; Li et al., 2004; Phillips and Reeves, 2001; Scheff et al., 2005). In neocortex, growth-associated protein-43 (GAP-43, a marker of axonal growth) does not increase, at least within 21 days post-CCI (Thompson et al., 2006), and synaptic proteins, such as post-synaptic density protein 95 (PSD-95), synapse-associated protein-07 (SAP-07), and synapsin I, decrease in a time-dependent manner out to 96 h post-CCI (Ansari et al., 2008b). These instances of decreased plasticity following TBI may be related to the upregulation of inhibitory molecules such as Nogo-A. Following fluid percussion injury (FPI), Marklund and associates (2006) found that Nogo-A is significantly increased in cortical neurons and glia of the injured hemisphere from days 1–7 after FPI (the contralateral cortex was not examined). Although some markers of plasticity and its inhibitors have been examined in animal models of TBI, neocortical dendritic arborization and the contralateral changes seen following CCI have not been examined in detail. Thus, it remains unclear whether the behaviorally relevant compensatory plasticity evident in other injury models could contribute to functional outcome after TBI. The current study was designed to examine whether structural neuroplasticity occurs in both the cortex surrounding injury and in the contralateral homotopic cortex following a unilateral CCI to the FL-SMC, and to investigate its temporal relationship with behavioral changes.

Methods

Subjects

Fifty-six adult male hooded Long-Evans rats (275–375 g) from Charles River Laboratories were used. The animals were assigned randomly to CCI and sham conditions and to histological end-points. All rats were treated according to institutional and National Institutes of Health guidelines, fed *ad libitum*, and group housed on a 12-h:12-h light/dark cycle at DePaul University.

Controlled cortical impact

A unilateral CCI was administered using modified procedures (Sutton et al., 1993). Once anesthetized with Equithesin (149 mg/100 g chloral hydrate and 31 mg/100 g sodium pentobarbital IP), the animals received a 4-mm-diameter craniotomy 0.5 mm anterior and 4 mm lateral to the bregma, directly over the FL-SMC, and centered over the primary motor and sensory overlap zone of the caudal forelimb area (Donoghue, 1982). The cortical impact was delivered by a small-bore, double-acting, pneumatic piston cylinder with a 40-mm stroke mounted on a stereotaxic micro-manipulator (David Kopf Instruments, Tujunga, CA). The pneumatic piston cylinder was angled 18° away from vertical, placing the flat impactor tip (3 mm in diameter) perpendicular to the surface of the brain. Once in place, the impactor tip penetrated the exposed brain at 0.3 m/sec at a depth of 2.3 mm below the cortical surface for 250 msec. After the impact, the wound was sutured and topical analgesics and antibiotics were applied. The animal was placed in its home cage and kept warm to recover from anesthesia prior to being returned to the DePaul University Animal Facility. Sham animals received all procedures up to but not including the craniotomy.

Behavior

The rats were tested on the foot-fault and limb-use tests on day 0 (pre-injury) and days 2, 4, 7, 10, 14, 21, and 28 post-injury, or until their assigned histological end-point.

Foot-fault test. Foot-fault is a measure of forelimb coordination during locomotion (Hernandez and Schallert, 1988). The rats were placed on a grid (33.02 × 25.40 × 7.62 cm with 2.54-cm openings). The number of left and right forelimb faults was counted over 50 steps. A fault consisted of the animal's forelimb completely falling through the space on the test tube rack. A step was counted when both the left and right forelimb moved consecutively in one direction. Foot-fault data are presented as: [(contralateral (to the injury) fault – ipsilateral fault)/total steps] × 100.

Limb-use test. The use of forelimbs for natural exploratory behavior was examined by placing the rats in a clear acrylic glass cylinder, and videotaping them for at least 2 min or until 10 rear-before-wall movements were completed (Kozlowski et al., 1996). The videotapes were analyzed and data measuring the use of forelimbs for weight-bearing exploratory behaviors such as rearing, landing, and exploring the walls of the cylinder were collected. If the animals failed to meet the criterion of making 10 rear-before-wall movements, they were excluded from the analysis on that testing day. No sham animals failed to meet the criterion on any testing day, but some CCI animals did at each post-injury time point ($n = 4$ on day 4, $n = 1$–2 on the remaining testing days). The total number of ipsilateral and contralateral (to the CCI) forelimb behaviors was obtained, and a percent use of the ipsilateral (non-injured) forelimb was calculated. Limb-use data are presented as %(ipsilateral limb use + 1/2 bilateral use)/total forelimb use).

Histology

Rats were euthanized on days 3, 7, 14, or 28 post-injury ($n = 8$–12 per group) by cardiac perfusion with 4% buffered paraformaldehyde in phosphate-buffered saline (PBS) while under Equithesin anesthesia (149 mg/100 g chloral hydrate and 31 mg/100 g sodium pentobarbital IP) for histological preparations. Sham animals were sacrificed on day 3 or 28 after sham surgery. The brains were removed, cryoprotected, and stored at 4°C until sectioning. The brains were sectioned rostrally to caudally in 50-μm coronal serial sections using a vibratome. Seven rostral-caudal sets of equidistant sections were produced. Six sets were placed in cryoprotectant and one set was used for each histochemical labeling procedure. Each seventh section was placed in PBS for immediate slide mounting, and this set was stained with toluidine blue (0.25%; Sigma-Aldrich, St. Louis, MO), a Nissl stain, and used for the analysis of remaining cortical volume (an indirect measure of contusion size). All tissue quantification was performed in a manner blinded to the post-surgical time point.

Measurement of remaining cortical volume

Measurements of cortical volume were obtained to estimate contusion size by visualizing Nissl-stained sections of the FL-SMC region using a Leica Microscope and cooled CCD camera at 2.5×. The images were analyzed using the computer program Neurolucida (MicroBrightfield, Colchester, VT). Sections between approximately 2.7 mm anterior to the bregma and 2.7 mm posterior to the bregma were chosen. After calibrating the software, a contour was drawn around the remaining cortex of the injured hemisphere of the brain using a low-power objective and an area was obtained. For sham animals a random hemisphere was chosen. The area of remaining cortex for all sections was summed per animal. A total cortical volume was obtained by multiplying the total cortical area by the distance between successive sections in the set (350 μm).

Immunohistochemistry

Immunohistochemical processing for MAP-2, SYN, and Nogo-A was performed in adjacent sets of sections, as in previous studies (Adkins et al., 2004; Hsu and Jones, 2006). Following rinses in 0.01 M PBS and inactivation of endogenous peroxidase activity with 0.3% hydrogen peroxide in PBS, the slices were incubated for 2 h in a block solution of 0.2–0.4% Triton X-100, 0.1% bovine serum albumin, and 2% horse (MAP-2 and SYN) or goat (Nogo-A) serum in PBS to prevent non-specific protein binding. The sections were rinsed in PBS again and placed in 1:500 mouse monoclonal anti-MAP-2 (2a + 2b, clone AP-20; Sigma-Aldrich), 1:200 mouse monoclonal anti-SYN (clone SVP-38; Sigma-Aldrich), or 1:200 rabbit polyclonal anti-Nogo-A (H-300; Santa Cruz Biotechnology, Santa Cruz, CA) in block solution for 48 h at 4°C. The sections were rinsed in PBS and placed in a 1:200 dilution of secondary antibody (horse anti-mouse for MAP-2 and SYN, goat anti-rabbit for Nogo-A) in PBS with 2% serum for 1 h. After more PBS rinses, the sections were placed in biotinylated horseradish peroxidase-avidin complex (Vectastain ABC kit; Vector Laboratories, Burlingame, CA) for 2 h. Finally, immunoreactivity was visualized using 3-3′-diaminobenzidine and nickel ammonium sulfate. Per each antibody, sections from all brains of the study were processed in one batch, to avoid batch-to-batch variability. To test for nonspecific binding, each batch contained a few control slices that were not exposed to the primary antibody.

Sampling strategy for MAP-2, SYN, and Nogo-A quantification

In the injured hemisphere, the focus of the quantification was layer V of the remaining cortex medial and lateral to the contusion (containing the remaining motor and somatosensory cortex). In the contralateral hemisphere, the focus was the cortical region homotopic to the injury. Neuronal structural plasticity in these regions has been linked with functional outcome (Adkins et al., 2006; Brown and Murphy, 2008; Carmichael and Chesselet, 2002), and behavioral asymmetries (Adkins et al., 2004; Hsu and Jones, 2006), after similarly placed ischemic lesions. The forelimb region of the sensorimotor cortex (SMC) includes agranular cortex (containing the primary motor cortex), granular cortex (containing the primary somatosensory cortex), and the overlap zone between them. These subregions have distinct cytoarchitectural characteristics (Wise and Donoghue, 1986), and consistent locations relative to macrostructural landmarks, and both were used to guide sample location, as described previously (Chu and Jones, 2000; Jones, 1999). Systematic random sampling (i.e., sampling at fixed increments but with a random start point; Gundersen and Jensen, 1987; Madow and Madow, 1944) was used to select sample locations, as in previous studies (Adkins et al., 2004; Hsu and Jones, 2006; Jones, 1999). The coronal sections sampled were between 1.2 mm anterior and −0.3 mm posterior to the bregma. The most anterior section sampled within this region was randomly selected (as a result of random selection of one of the seven equidistant section sets per immunohistochemical stain), with sections subsequently sampled at fixed 350-μm distances in the posterior direction. Per each section, the first sample location was positioned randomly in the depth of layer V within an increment distance relative to the medial edge of the FL-SMC of intact hemispheres, or to the edges of the contusion in injured hemispheres. Subsequent samples were taken at fixed increments moving parallel to cortical laminae. A computer-interfaced Nikon Optiphot 2, a high-resolution digital camera with live imaging capability (DVC Inc., Austin, TX), a rotating stage permitting alignment relative to the laminae, and a digital micrometer measuring stage movement were used.

MAP-2-labeled dendritic surface density analysis

The cycloid-grid intersection method (Baddeley et al., 1986) was used to estimate the surface density of dendritic processes immunostained with MAP-2, as described previously (Adkins et al., 2004). Four samples in each of three sections in both hemispheres (24 samples per brain) were observed, moving in 200-μm increments between samples within sections. A cycloid-grid reticle was placed in one of the eyepieces. Each sample site was viewed using a 100× oil-immersion objective (n.a. 1.30, 1250× final magnification), and intersections between the cycloid grid lines and MAP-2-immunoreactive processes were counted. Out-of-focus processes were not counted to minimize projection bias, as appropriate for the cycloid method. The vertical axis of the cycloid arcs was perpendicular to the cortical surface and parallel to apical dendritic shafts (i.e., aligned using local vertical windows;

Baddeley et al., 1986). Immunoreactive somata were not included in the measures. Surface density (Sv) was calculated using the formula: $Sv = 2(I/L)$, where I is the total number of intersections summed across all samples per hemisphere, and L is the total cycloid test line length, summed over samples (2.75 mm).

SYP optical density quantification

SYP-immunostained sections were viewed using a 100× oil-immersion objective for a final magnification of 2800×. Digital images were captured and the luminosity of the sample was obtained using DVC View 3.3 software. Microscope and illumination settings were held constant. Eight samples taken at 200-μm increments were imaged per hemisphere in each of three sections (48 samples/brain). Luminosity was recorded from the midline of the corpus callosum to serve as a background measurement. A blank area of the slide near the midline of the coronal section was also sampled to verify constancy of background illumination. The luminosity measures reflect both in- and out-of-focus labeling. The optical density (the inverse of luminosity) for each hemisphere was calculated as the average optical density of sample areas/optical density of the corpus callosum.

Nogo-A quantification

The numerical density of Nogo-A-immunolabeled cells was estimated using the optical disector method. Samples were viewed with a 50× oil-immersion objective (1400× final magnification), and viewed in real time on a computer monitor using DVC View 3.3 software. Four samples per each of 4 sections and in each hemisphere (32 total/brain) were taken at 250-μm increments. An unbiased sample frame (30,000 μm^2) was superimposed over the image. Labeled cells appearing while focusing down through the thickness of the section were counted, whereas cells at the top focal plane were excluded. The numerical density (Nv) was calculated as $\sum$Q-/$\sum$V(frame) where $\sum$Q- is the total number of Nogo-A-positive cells per hemisphere, and $\sum$v(frame) is the summed sample volume (24×10^6 μm^3). Cells that had an obvious neuronal morphology, characterized by large pyramidal-shaped soma, and often a portion of the apical dendrite, were counted separately from other cells. This method of morphological phenotyping benefits from the large size and distinctive morphology of the principal neurons of layer V. Counterstaining with pyronin-Y (a Nissl stain) after data collection verified that the nuclei of cells appearing to have neuronal morphology with Nogo-A labeling also had the distinct spherical nucleoli characteristic of neurons, and an absence of the chromatin clumping or dark staining characteristic of glia (Peters et al., 1991). This approach is likely to omit smaller and necrotic neurons. Thus, the "other cell" category is expected to include some small neurons as well as non-neuronal cells.

Fluoro-Jade B stain

Another set of tissues was stained for FJB (Chemicon, Temecula, CA), a polyanionic fluorescein derivative that binds to deteriorating neurons (Schmued and Hopkins, 2000). The manufacturer's protocol for FJB staining was used. As described previously (Adkins et al., 2006), gelatin-coated slides with mounted tissue were immersed in a solution of 1% sodium hydroxide in 80% alcohol for 5 min, and 70% alcohol for 2 min, distilled water for 2 min, and 0.06% potassium permanganate for 30 min on a shaker table. The rest of the steps were conducted away from direct light. The slides were placed in a solution of 0.0004% FJB in distilled water for 30 min. After several rinses with distilled water, the slides were dried overnight, placed in xylene for 5 min, and coverslipped with Krystalon mounting media (EMD Chemicals, Inc., Gibbstown, NJ).

FJB analysis

FJB-positive neurons in the peri-lesion FL-SMC were counted and averaged from three sections as described by Adkins and colleagues (2006). The sections were viewed in real time on a computer monitor using an Olympus BX61 fluorescence microscope, Optronics Microfire digital camera (Meyer Instruments, Inc., Houston, TX), and Neurolucida software. At a lower magnification of 140×, the cortex of either hemisphere was outlined, and the area of the delineated region was determined using the Neurolucida program's area estimation function. Using a 20× dry objective (final magnification of 700×), the FJB-positive neurons observed within the previously outlined area of either hemisphere were counted. The use of an exhaustive sampling scheme within the stained cortex enabled detection of infrequent or scattered FJB-labeled neurons. The number of FJB-positive neurons per unit area was calculated as the total number counted divided by the area of the delineated cortical region.

Statistical analysis

The behavioral and histological data were collected from the same animals. For analysis of behavioral data, the removal of animals for histological end-points complicates the use of repeated-measures analysis of variance (ANOVA), because animal subsets and group sizes varied across the behavioral time course. Therefore, as a primary analysis inclusive of all animals, behavioral data were analyzed using individual ANOVAs for injury condition (CCI versus sham) at each testing day using SuperAnova software. To confirm the pattern of results, an additional analysis was performed using two-way ANOVA for injury condition (CCI versus sham) and time (testing day), using only data from animals surviving until the last end-point (day 28), and treating time as a repeated measure. In the first analysis, all surviving animals were included in the analysis of each testing day because within CCI and sham conditions, there were no significant differences at any behavioral time point between surviving end-point groups ($p = 0.09$–0.97). Anatomical variables were analyzed with R (R Development Core Team, 2010) using planned contrasts for time point, treating sham-operated animals as "day 0" for comparison with each post-CCI time point (i.e., four planned contrasts per variable). For the latter analysis, the R gmodel package and fit.contrast procedure were used to generate one-way ANOVAs for time point, followed by the constructed contrasts. Select secondary *post-hoc* analyses comparing time points among CCI groups were performed using Tukey's HSD testing. Data from the two time points (days 3 and 28) and hemispheres of sham-operated animals were combined for most analyses, because preliminary analyses revealed no significant differences between these for any of the anatomical variables

[$F_{(1,14)} = 0–0.31$, $p = 1.0–0.59$], with the exception of one sub-analysis of the Nogo-A results, as considered below. The results were considered significant at $p \leq 0.05$. Graphed data are shown as means ± standard error of the mean (SEM).

Results

Remaining cortical volume

There was a significant reduction in the volume of the injured SMC compared with sham-operated animals [$F_{(1,52)} = 43.43$, $p < 0.0001$; Table 1). The mean remaining cortical volume tended to decline across time points. However, in *post-hoc* Tukey's HSD comparisons there were no significant differences in remaining cortical volume between CCI groups at the different time points ($p = 0.17–0.99$). It is possible that the tendency for a progressive decline in cortical volume reflects progressive tissue loss and atrophy rather than differences in initial contusion size. Consistent with this, initial behavioral impairment levels were similar between rats sacrificed at different time points after CCI. For example, considering rats sacrificed at 3 versus 28 days after CCI, there were no significant differences in any of the early behavioral measures between these CCI subgroups (e.g., foot-fault: [$F_{(1,19)} = 0.146$, $p = 0.79$]).

Behavior

Foot-fault test. Intact animals had very few foot-faults across all of the testing days. All CCI animals showed an increase in the number of contralateral (to the contusion) foot-faults starting at day 2 post-injury compared to sham animals [$F_{(1,53)} = 90.13$, $p < 0.001$; Fig. 1), indicating a deficit in motor coordination of the forelimb contralateral to the CCI. The deficits began to recover over time in CCI animals. Nevertheless, at the end of the study, the injured animals were still showing significantly more contralateral foot-faults compared to sham animals [$F_{(1,16)} = 13.75$, $p < 0.001$]. Similar effects were found in a separate analysis including only animals that survived until the last end-point (day 28). In these subgroups, two-way repeated-measures ANOVA revealed a significant main effect of injury condition [CCI versus sham, $F_{(1,18)} = 74.84$, $p < 0.001$], and condition × day interaction [$F_{(6,108)} = 2.30$, $p = 0.040$]. In *post-hoc* comparisons, CCI was significantly different from sham animals at each post-injury time point, but tended to be more impaired at earlier time points. These results demonstrate that the CCI produces deficits in the motor coordination of the forelimb contralateral to the injury, as is seen in electrolytic lesions and ischemic injury to the FL-SMC (Adkins et al., 2004; Kozlowski et al., 1996).

Table 1. Volume of the Remaining Cortex

Group	*Volume of remaining cortex (mm^3 ± SEM)*
Sham	59.2 ± 1.2
CCI, day 3	50.4 ± 2.2*
CCI, day 7	45.6 ± 2.3*
CCI, day 14	45.2 ± 2.3*
CCI, day 28	43.9 ± 2.2*

*$p < 0.05$ compared to sham animals.
CCI, controlled cortical impact; SEM, standard error of the mean.

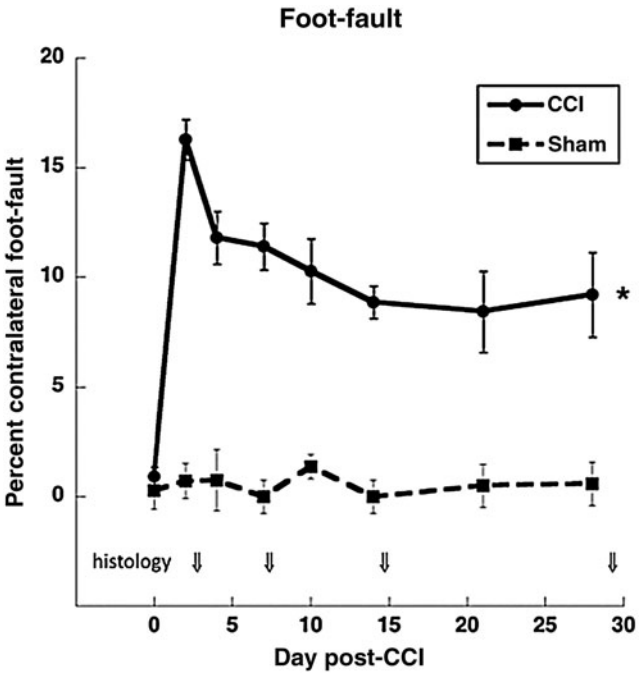

FIG. 1. Foot-fault test. All injured animals showed a deficit in forelimb coordination that recovered over time compared to sham animals (*$p < 0.05$ at all time points). Arrows indicate times when animals were removed for histological end-points. Numbers of controlled cortical impact (CCI) animals: days 0–2 = 41, days 4–7 = 31, days 10–14 = 21, days 21 and 28 = 9 and 10. Numbers of sham animals: days 0–2 = 14, all other days = 8.

Limb use: Schallert cylinder test. Intact animals had a forelimb asymmetry score of approximately 50%, which indicates symmetrical use of both forelimbs (Schallert et al., 1997). All CCI animals showed an increase in cylinder forelimb asymmetry scores starting at day 2 post-injury, indicating enhanced reliance on the non-impaired forelimb compared to sham animals [$F_{(1,51)} = 32.6$, $p < 0.0001$; Fig. 2]. CCI animals were significantly different from sham animals at each time point, with the exception of day 28 [$F_{(1,16)} = 2.85$, $p = 0.10$]. In two-way ANOVA inclusive of animals of the final end-point, there was a significant main effect of injury condition [CCI versus sham, $F_{(1,17)} = 17.87$, $p = 0.001$], but no injury condition × day interaction [$F_{(6,102)} = 1.29$, $p = 0.27$]. These results demonstrate that the CCI does produce a significant asymmetry in the use of the forelimbs during weight-bearing exploration, as is seen in electrolytic lesions and ischemic injury to the FL-SMC (Adkins et al., 2004; Kozlowski et al., 1996).

Anatomy results

Changes in MAP-2-labeled dendrites following CCI. After CCI, there was a major reduction in the surface density of MAP-2-labeled dendrites in cortical layer V. The decreases in dendritic density were found bilaterally at most time points examined (Fig. 3). One-way ANOVA for time points, treating sham animals as day 0, revealed significant time-dependent differences in both the injured [$F_{(4,51)} = 11.49$, $p < 0.00001$] and intact [$F_{(4,51)} = 4.76$, $p = 0.002$] hemispheres. MAP-2-labeled dendrites were sparsest in the injured hemisphere at 3 and 14

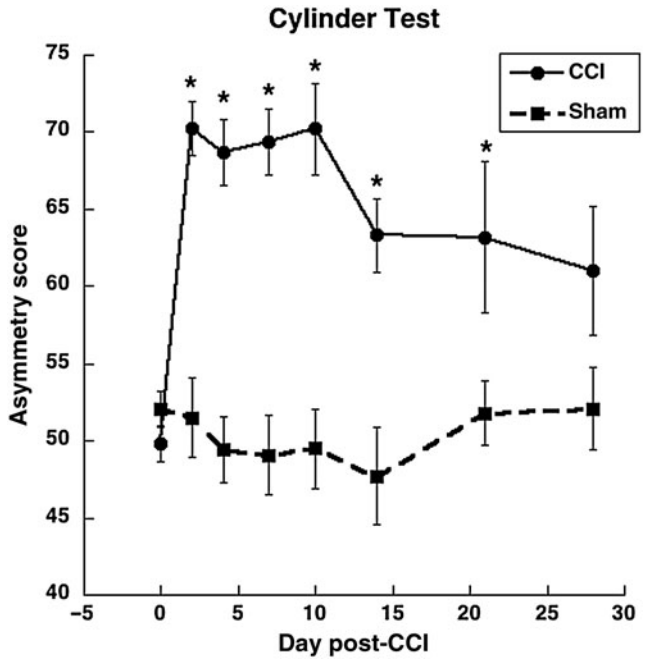

FIG. 2. Cylinder test. All injured animals showed a preferential reliance on the non-impaired forelimb for postural support as measured by the asymmetry score: [{(ipsilateral use + ½ bilateral use)/total use} * 100]. Numbers of controlled cortical impact (CCI) animals: days 0 and 2 = 41 and 39, days 4 and 7 = 26 and 30, days 10 and 14 = 21 and 20, days 21 and 28 = 9 and 10. Numbers of sham animals: days 0 and 2 = 14, 8 for all remaining time points (*$p < 0.05$ compared to sham animals).

days after CCI. At these times, there were approximately 27% and 32% reductions in dendritic densities, respectively, compared with sham animals (t = 4.98 and 6.03, respectively; $p < 0.00001$). A similar pattern of results was found in the contralateral cortex, though the reductions in this hemisphere were not as extreme. Neither hemisphere showed unequivocal evidence of successful recovery of dendritic density over the time course examined. Though there was a partial return to more normal dendritic density at days 7 and 28, at day 14 the mean dendritic density was at its lowest in both hemispheres. Furthermore, dendritic densities remained significantly reduced 28 days after CCI in both the injured (t = 2.98, $p = 0.004$) and contralateral (t = 2.94, $p = 0.005$) hemispheres in comparison to sham animals.

Changes in synaptophysin immunoreactivity following CCI. The optical density of SYN showed a time-dependent elevation in the injured cortex, but did not change significantly in the contralateral cortex (Fig. 4). In the injured hemisphere, there was an overall effect of post-CCI time point [$F_{(4,49)} = 2.64$, $p = 0.045$, including sham as day 0]. At 3 and 7 days after CCI, mean SYN optical densities were similar to those of sham animals. However, on day 14, SYN optical density was ~ 28% greater than that of sham animals (t = −3.01, $p = 0.004$). Qualitatively, the labeling pattern in the injured cortex on day 14 was characterized by regions of dense and atypically clustered puncta (Fig. 4A), in contrast to the diffusely distributed puncta typical of intact and contralateral cortex (Fig. 4B). On day 28 after CCI, mean values remained slightly elevated, but were not significantly different from shams (t = −1.41, $p = 0.17$). Though the contralateral cortex tended to mirror the injured hemisphere's temporal pattern of change, the changes were subtle and there was no overall effect of time in the one-way ANOVAs for this hemisphere [$F_{(4,49)} = 1.45$, $p = 0.23$]. There were also no significant differences between sham animals and any of the post-CCI time points in the contralateral cortex. Note that increases in SYN labeling do not necessarily reflect increased synaptic densities, as they can also reflect disrupted transport and pathological accumulation of the protein (Ferrer, 2002; Jortner et al., 1997; Tesseur et al., 2000).

Neuronal degeneration following CCI. FJB analysis was conducted to examine neuronal degeneration in both hemispheres over time. As shown in Figure 5, there were major increases in FJB-labeled neurons in the cortex near the CCI. The clearly labeled FJB-positive neurons evident in the injured cortex (Fig. 5A and B) were not found in sham animals or in the hemisphere contralateral to the injury (Fig. 5C). As shown in Figure 5D, degenerating neurons were most abundant early after injury, and declined with time [ANOVA for time, including shams as day 0: $F_{(4,47)} = 5.34$, $p = 0.0013$]. The density of degenerating neurons was greatest 3 days after CCI, and this was significantly increased compared with shams (t = −4.15, $p = 0.0001$). The mean FJB-positive cell densities at post-CCI days 7 and 14 remained elevated, but failed to reach significance compared with shams ($p = 0.093$ and 0.0502, respectively). Finally, neurodegeneration labeling was minimal at post-CCI day 28, and did not significantly differ from the sham group (t = −0.04, $p = 0.97$).

Expression of Nogo-A following CCI

Nogo-A labeling was conducted to examine whether the failure to recover dendritic density may have been related to the upregulation of inhibitory molecules such as Nogo-A. Changes in Nogo-A-labeled cell densities after CCI showed bidirectional effects dependent upon cell morphological category. As shown in Figure 6, the densities of other Nogo-A-positive cells (those without a clear neuronal morphology) were increased at all time points examined. In contrast, Nogo-A-positive cells with a neuronal morphology were significantly reduced in the injured hemisphere. This reduction was significant compared with shams at all time points examined, though there was a partial return to sham levels at day 28 after CCI. In *post-hoc* comparisons between CCI groups, densities of Nogo-A-positive cells with neuronal morphology were significantly greater at day 28 than on days 3 ($p = 0.014$) and 7 ($p = 0.011$ by Tukey's HSD) post-CCI. Levels on day 14 were not significantly different from either earlier or later time points.

In the contralateral cortex, there was little change in Nogo-A labeling of cells categorized as neurons or other cells. There were no significant differences between the CCI and sham groups at any time point, with the exception of a significant decline in Nogo-A-positive cells with a neuronal morphology at 3 days after CCI (t = 2.28, $p = 0.027$).

Neuronal death is unlikely to account for the reduced densities of Nogo-A-positive cells with a neuronal morphology. There was no evidence of neuronal death in the

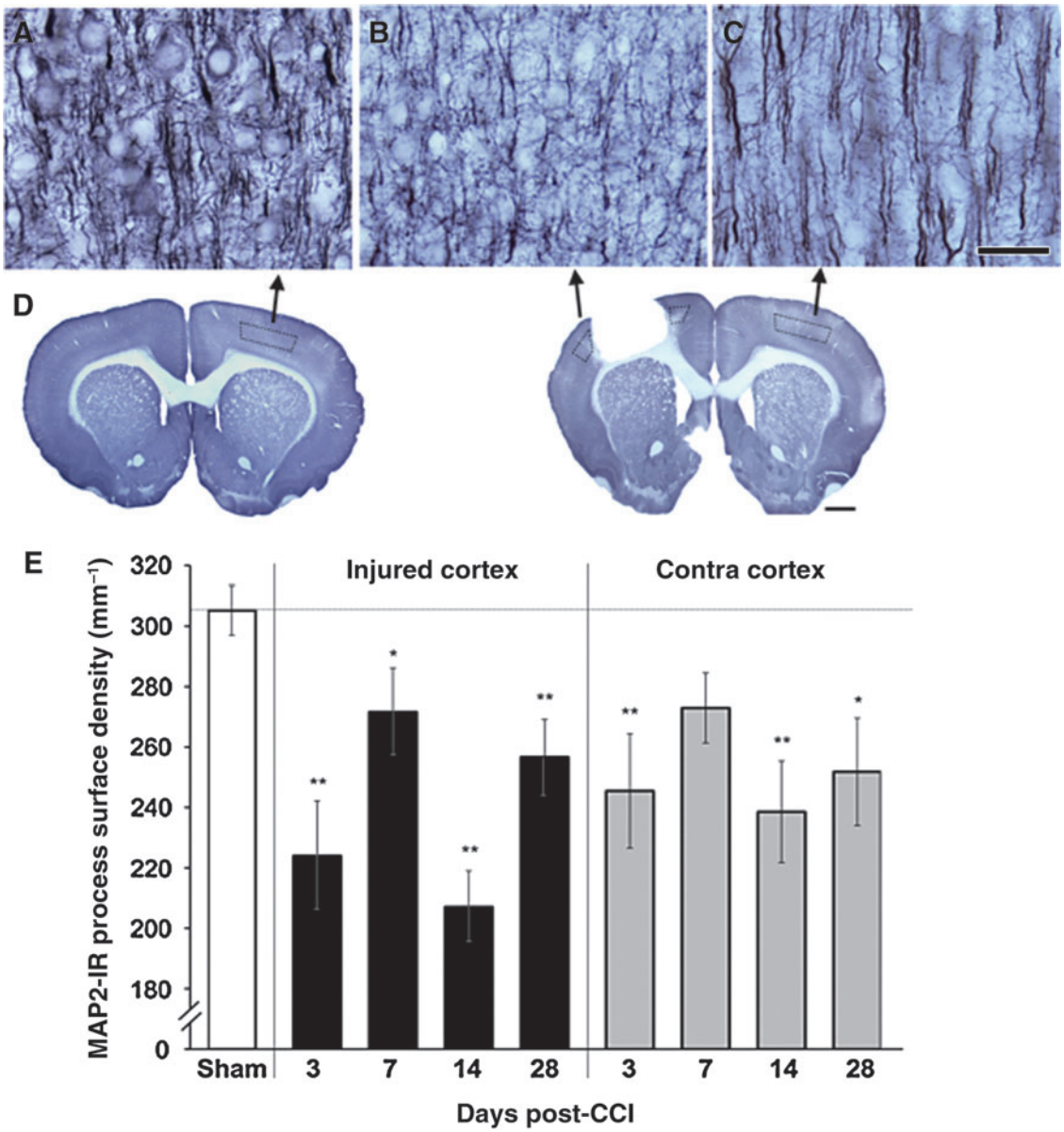

FIG. 3. The density of dendritic arbors (microtubule-associated protein-2, MAP-2) in layer V (**A**–**C**) were decreased surrounding the injury (**B**), and in the contralateral homotopic cortex (**C**), compared to sham animals (**A**; scale bar = 50 μm). Layer V sampling regions are outlined in the coronal sections in (**D**; scale bar = 1 mm). (**E**) These decreases were seen at all time points following controlled cortical impact (CCI; *$p < 0.05$, **$p < 0.005$ versus sham animals in planned comparisons; at day 7 in the contralateral [Contra] cortex, $p = 0.08$ versus sham animals). Color image is available online at www.liebertonline.com/neu

contralateral cortex to accompany the reduced densities of these cells at 3 days. In addition, a persisting reduction in neuronal Nogo-A densities (possibly with a more delayed onset) would be expected in the injured hemisphere, rather than the early peak reduction followed by partial recovery that was observed. Our approach for categorizing cells would count small and necrotic neurons as "other cells." However, if dying neurons contributed to the elevations in the "other cell" category in the injured cortex, these densities would be expected to decline after neuronal degeneration peaks (see FJB results), and degenerating debris is removed. In contrast, there was no reduction with time in the density of other Nogo-A-positive cells in the injured hemisphere.

For all other anatomical measures, there were no differences between the two time points of sham animals. However, in the measure of Nogo-A-positive cells with neuronal morphologies, sham animals at day 3 had significantly greater densities than those at day 28 [3.40 ± 0.50 and 2.19 ± 0.31, respectively, $F_{(1,14)} = 4.86$, $p = 0.045$]. However, if animals with the most extreme values from each group were omitted, such that groups were no longer significantly different, there was no change in the pattern of inferential results in the comparison with CCI groups. Furthermore, if CCI groups are compared only with the day-28 sham group (which had lower neuronal cell densities), there continued to be significant CCI versus sham effects at all but the last time point (days 3–14: $p = 0.002$–0.009, day 28: $p = 0.26$).

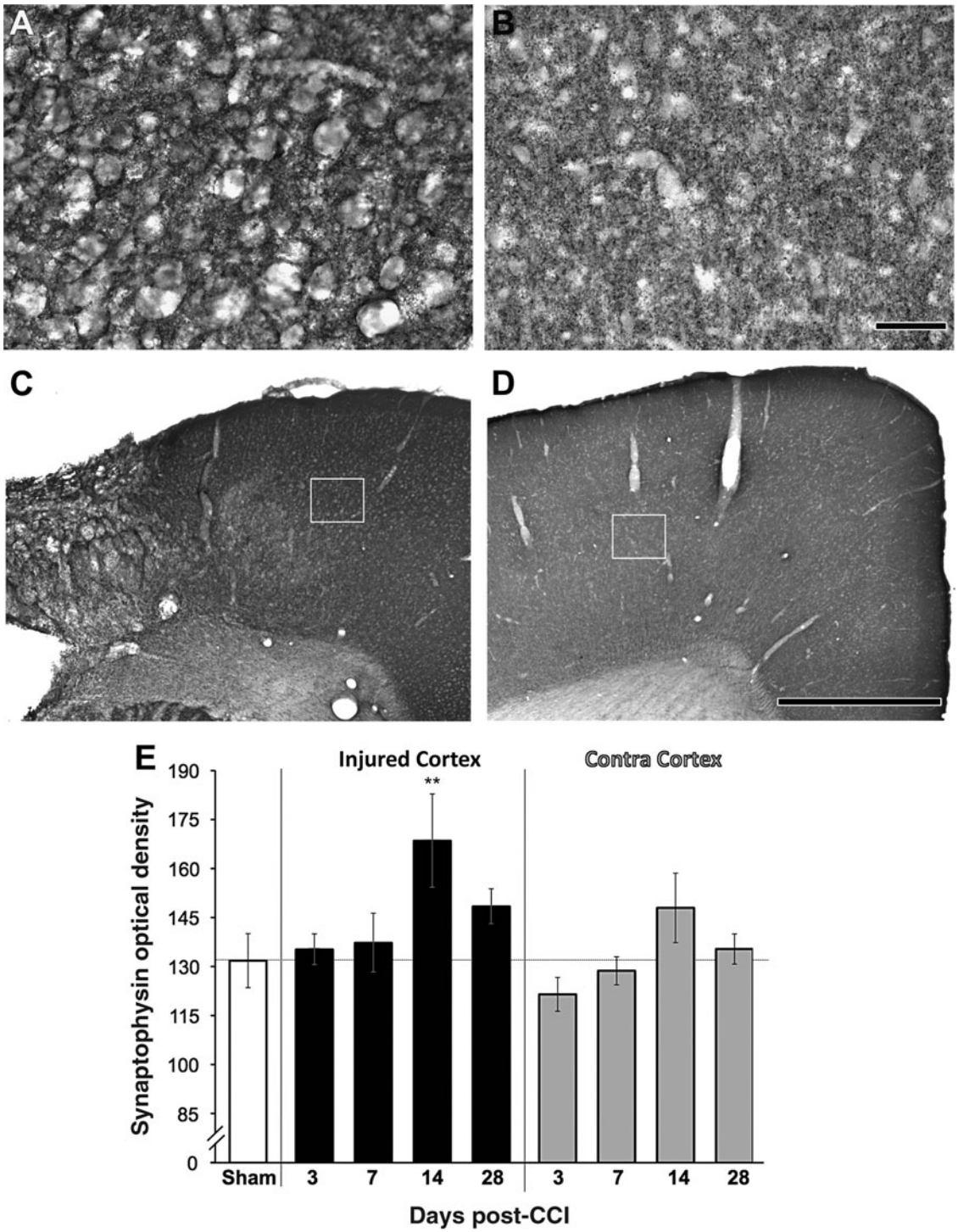

FIG. 4. Synaptophysin (SYN) immunolabeling in cortex near a controlled cortical impact (CCI; **A**), and in the contralateral cortex (**B**; scale bar = 50 μm). The white boxes in **C** and **D** delineate the regions shown in the higher-magnification images seen in **A** and **B**, respectively (scale bar = 1 mm). (**E**) In the injured cortex, there was a transient increase in the optical density of SYN on day 14. No significant changes were found in the contralateral (Contra) cortex (**$p = 0.004$ versus sham animals).

Discussion

Neuroplasticity has been established as one of the mechanisms enabling functional improvements following CNS injury (Kleim and Jones, 2008). It can be behaviorally driven by both rehabilitative training and by an animal's "self-taught" compensatory behavioral strategies. An example of the latter category is found in the cortex contralateral to a unilateral ischemic FL-SMC, where increased reliance on the unimpaired forelimb can drive dendritic growth and synapse addition. In the current study, we probed for similar behaviorally-driven cortical structural plasticity over time

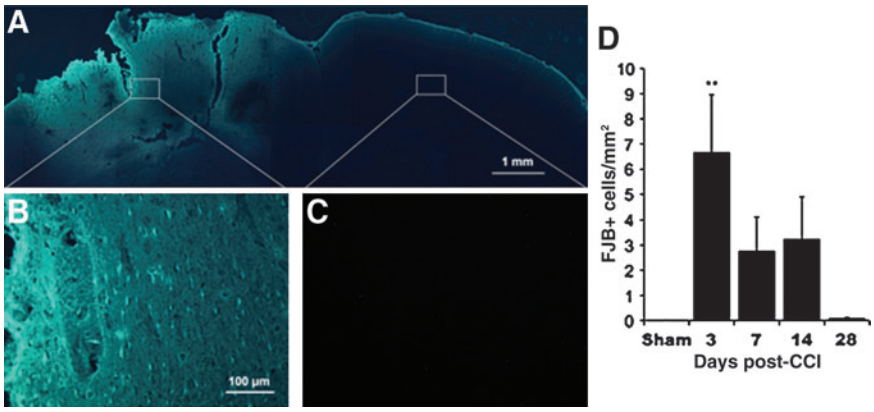

FIG. 5. Fluoro-Jade B (FJB) labeling for degenerating neurons. (**A–C**) Representative images from 3 days post-CCI. (**A**) Photomontage of the dorsal portion of a coronal section overexposed to reveal cortical outlines. White boxes outline areas shown in the higher-magnification images seen in **B** (injured hemisphere) and **C** (contralateral cortex). (**D**) Quantification of the density of FJB-labeled neurons. Significant increases were found in the injured cortex at 3 days post-CCI (**$p < 0.005$ versus shams; CCI, controlled cortical impact). Color image is available online at www.liebertonline.com/neu

following focal contusion injury of the FL-SMC produced by a CCI. Our findings indicate that, although unilateral CCI produced significant deficits in forelimb function and increased reliance on the unimpaired limb (similar to what is seen following a similarly sized and placed ischemic or electrolytic lesion to the FL-SMC), structural plasticity is compromised. There was a major loss of dendrites in both hemispheres that endured across the entire time course examined in this study. If there was any re-growth of dendrites, it was far from sufficient to restore their quantities in the cortex of either hemisphere to normal levels by 28 days after CCI.

Unilateral CCI to the FL-SMC produced significant deficits in motor coordination of the forelimb contralateral to the injury, as well as a reliance on the unimpaired limb during weight-bearing exploratory movements. These deficits and forelimb asymmetries did not fully recover over time. The deficits were similar to those previously reported after CCI of the caudal forelimb area of the SMC (Becerra, 2007; Hoane et al., 2007; Nishibe et al., 2010). The severity and extent of the deficits and asymmetrical forelimb use were also similar to those found using the same measures following electrolytic (Kozlowski et al., 1996) or focal ischemic lesions of the FL-SMC (Hsu and Jones, 2006), both of which result in significant post-lesion neuronal growth responses. Therefore, differences in growth responses between the present CCI TBI model and electrolytic and ischemic lesions cannot easily be explained by differences in forelimb deficits and asymmetries.

Dendritic density (as measured by the surface density of MAP-2-positive processes) was significantly decreased in both the injured cortex and in the contralateral homotopic cortex following CCI at most time points examined. There was no unequivocal evidence for successful recovery of dendritic densities. There were transient fluctuations in mean dendritic densities, but whether this reflects the failure to stabilize newly formed dendrites, or it reflects inter-animal variability in dendritic loss, requires further investigation. In either event, dendritic densities remained drastically reduced at all time points out to 28 days. These data are generally consistent with previous studies finding decreased MAP-2 immunoreactivity in both the hippocampus and in the cortex in different models of TBI (e.g., impact acceleration, weight drop, and fluid percussion; Folkerts et al., 1998; Huh et al., 2003; Posmantur et al., 1996; Taft et al., 1992). The majority of these studies found drastic decreases in MAP-2 surrounding the injury and in the hippocampus ipsilateral to the injury; however, these measurements were primarily taken within the first 3 days post-injury surrounding the injury and not in the contralateral homotopic cortex. Studies examining long-term effects of TBI on dendritic morphology have not been conducted. Therefore, our findings that dendritic density is decreased not only at the early post-injury time points, but chronically out to 28 days post-injury in both hemispheres, are novel and suggest that CCI results in widespread lasting structural degradation of surviving neurons in the cortex that is not compensated for by neuronal growth responses.

Our findings of chronic reductions in neocortical dendrites in the contralateral homotopic cortex are contrary to the pattern of dendritic changes seen after similarly sized and placed electrolytic and ischemic lesions, in which dendritic arborization in the contralateral cortex increases beyond control levels (Adkins et al., 2004; Jones and Schallert, 1992). However, as in TBI, these neuronal growth responses are very sensitive to the size and extent of damage (Hsu and Jones, 2006). In TBI models, markers of plasticity measured early post-injury are typically increased in more mild injury models like FPI, versus more severe models such as CCI (Hall and Lifshitz, 2010; Thompson et al., 2006). For example, expression of GAP-43 in the ipsilateral cortex following severe CCI is depressed (Thompson et al., 2006), whereas mild FPI results in increased GAP-43 expression out to 28 days post-injury (Hall and Lifshitz, 2010). In the current study, the injury produced by CCI would be categorized as moderate to severe, and therefore early decreases in plasticity markers would be consistent with the literature. Nevertheless, in focal stroke models, even though larger FL-SMC lesions diminish the magnitude of neuronal growth responses in the contralateral cortex compared with smaller lesions, there are still significant increases in the density of MAP-2-immunolabeled dendrites in this region (Hsu and Jones, 2006), in contrast to the persistent decreases found in the present study. The larger ischemic lesions induced by Hsu and Jones were of similar size

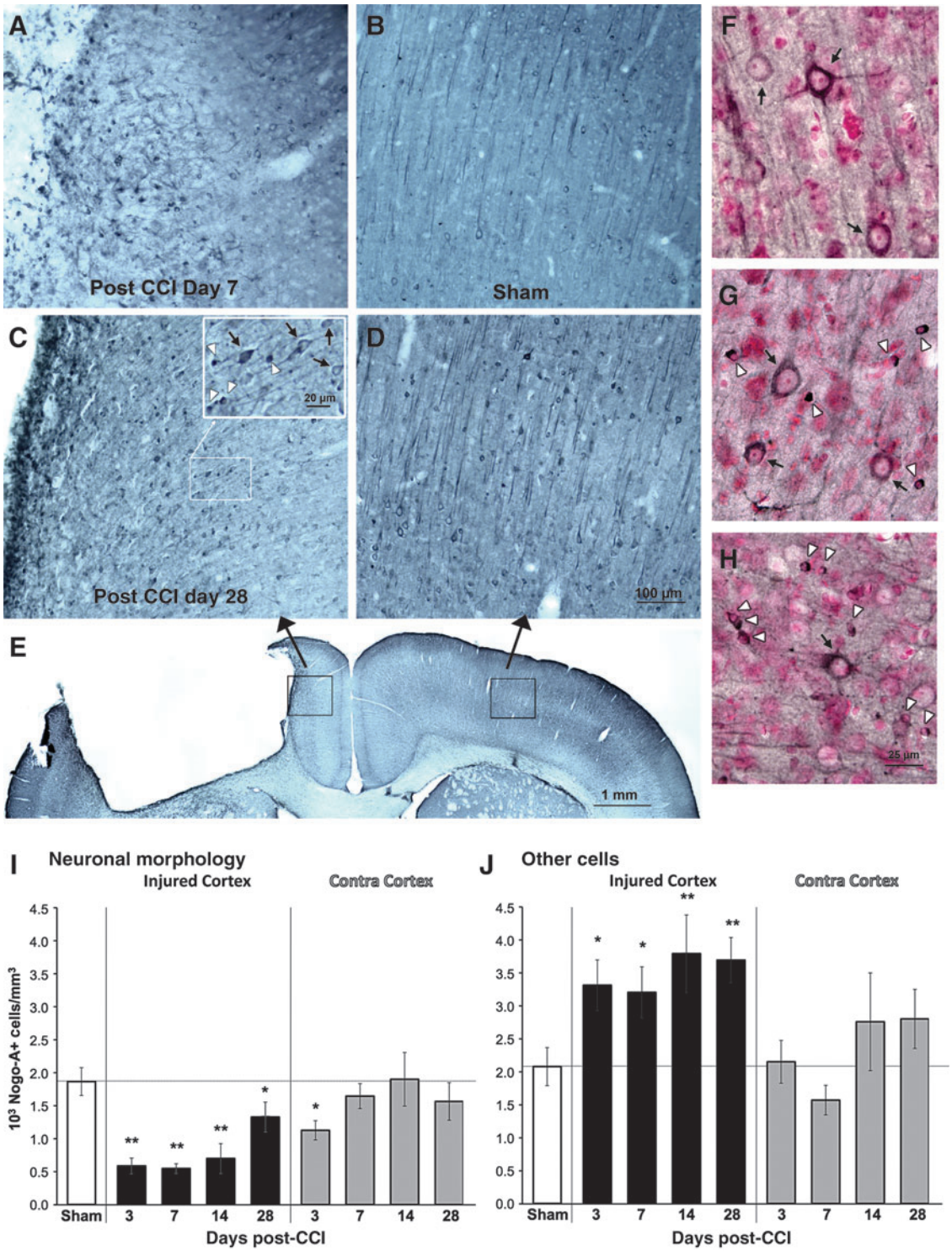

FIG. 6. Nogo-A labeled cortical samples from 7 days after controlled cortical impact (CCI, **A**), sham surgery (**B**), 28 days post-CCI (**C**), and contralateral cortex 28 days after CCI (**D**). The inset in **C** shows examples of cells categorized as having clear neuronal morphology (black arrows) or not (white arrowheads). (**E**) Lower-magnification view of the sample regions (black boxes) shown in **C** and **D**. Counterstaining with pyronin-Y (a Nissl stain) confirmed that cells with neuronal morphology had nuclei characteristic of neurons (**F-H**). Examples are from the contralateral cortex 28 days after CCI (**F**), the cortex lateral to the contusion at the same time point (**G**), and the cortex medial to the contusion on day 7 (**H**). In the injured hemisphere (**I**), there was a reduction in the density of Nogo-A-positive cells with obvious neuronal morphology, and an increase in other Nogo-A-positive cells, at all time points. In the contralateral (Contra) cortex (**J**), significant changes were only found at day 3 post-CCI, and only in Nogo-A-positive cells with neuronal morphology (*$p < 0.05$, *$p < 0.005$ versus sham animals). Color image is available online at www.liebertonline.com/neu

and extent as the CCIs in the current study (25% and 24% loss in cortical volume, respectively). Therefore, injury size alone cannot explain the difference in neuronal growth responses resulting from ischemic versus impact injury of the same cortical region.

In addition to differences in injury severity, the injury type also affects reactive plasticity. Dendritic and axonal growth responses to sensorimotor cortical damage have been found to vary between ischemic and electrolytic versus aspiration lesions (Carmichael and Chesselet, 2002; Mir et al., 2004; Voorhies and Jones, 2002). Dendritic processes grow in the contralateral cortex following an electrolytic or ischemic lesion, but not when the lesion is created by aspiration or a combined electro-aspiration technique (Voorhies and Jones, 2002). Although the mechanisms underlying these lesion-specific reactions have never been fully elucidated, one possibility is that aspiration procedures produce greater disruption of underlying brain structures, including white matter and striatum, which could promote greater inhibition of compensatory plastic changes. CCI is perhaps more like aspiration lesions than ischemic lesions in the severity and characteristics of its disruption of areas surrounding the area of impact along with white matter and connected subcortical structures (Dixon et al., 1991; Hall et al., 2008). Another potential mechanism is that ischemic lesions also produce patterns of synchronous cortical neural activity early post-lesion (1–3 days), which are not found following aspiration lesions. Blocking this activity after ischemic lesions prevents axonal sprouting (Carmichael and Chesselet, 2002). *In vitro* and *in vivo* studies have shown that electrophysiological responses and cellular excitability post-TBI are impaired (DeSalles et al., 1987; Reeves et al., 2000; Wiley et al., 1996). This impairment in cellular excitability post-TBI may prevent plastic structural changes. Further examination of these potential mechanisms is warranted.

The persistent reductions in dendritic densities seen in the contralateral cortex are unlikely to be due to a major loss of neurons in this region. While extensive neural degeneration (as measured by FJB labeling) was seen in the cortex surrounding the contusion in the current study, no FJB neuronal labeling was found in the contralateral cortex over the studied time period (3–28 days). Neurons may not be dying in significant numbers in this region, but major axonal degeneration in both the immediate and chronic stages post-CCI could be expected. Axonal damage is extensive following CCI, encompassing not just the injured hemisphere, but also the hemisphere contralateral to the injury (Hall et al., 2008). In an *in vitro* model of traumatic axonal injury (TAI), axonal degeneration caused by stretching results in an immediate effect on dendrites in the form of dendritic beading (Monnerie et al., 2010). This subsides *in vitro* once the stretch is discontinued. Therefore, the axonal stretching present following CCI can result in detrimental effects on dendrites, and may produce the subsequent decreases in dendritic density seen in this study and others. It is possible that even when tissue loss is similar, these characteristics of CCI result in more dire and extensive disruption and dysfunction of surviving neurons and circuitry than do ischemic lesions, compromising subsequent reactive plasticity in connected brain regions, including the contralateral cortex.

Compensatory plasticity also varies with metabolic responses to injury. Lesions that produce a longer hypometabolic state post-injury result in diminished compensatory plasticity (Mir et al., 2004). It is well known that following TBI, there is an intense early hypermetabolic response surrounding the injury, which quickly turns into a prolonged hypometabolic state (Hovda, 1996). The hypometabolic state can last at least 10 days post-injury, and has been correlated with deficits in performance in the Morris water maze (Moore et al., 2000). During this "metabolic crisis," the cortical response to both peripheral sensory (whisker) stimulation and direct cortical stimulation is significantly muted for up to 2 months post-injury (Ip et al., 2003; Passineau et al., 2000). The altered response to somatosensory activation occurs in the cortex of both hemispheres, and it is even more prolonged in the contralateral cortex (Ip et al., 2003). Thus, the cortical response to asymmetrical use of the forelimbs might also be diminished. These metabolic responses to injury have also been demonstrated following CCI (Kelly et al., 2000). Together, these findings raise the possibility that the compromised neuroplasticity seen following a CCI may be directly related to the compromised metabolic state and its associated reduction in cortical responsiveness to peripheral activation.

Another mechanism by which TBI may limit plasticity is by upregulating growth inhibitory molecules. A few inhibitors of plasticity in the cortex have been examined in animal models of TBI. Harris and colleagues found that the expression of the axonal growth inhibitor chondroitin sulfate proteoglycan (CSPG) in the cortex following CCI (Harris et al., 2009) is increased in areas surrounding the CCI that were forming a glial scar. In the pericontusional areas, however, there are decreases in CSPG proteins within the first 14 days post-injury. This suggests that the inhibition of plasticity may be more extensive surrounding the contusion in the glial scar, but that further away, decreases in inhibitory proteins could create an environment permissive for plasticity.

To our knowledge, our study is the first to examine the post-CCI response of the myelin-associated growth inhibitor Nogo-A (Chen et al., 2000; Grandpre et al., 2000; Zorner and Schwab, 2010), though a previous study has examined its expression patterns after FPI (Marklund et al., 2006). In the uninjured rat, Nogo-A is expressed in neurons and oligodendrocytes throughout the entire CNS (Funahashi et al., 2008), but not in astrocytes or activated microglia (Liu et al., 2002). In the sensorimotor cortex, Nogo-A expression is concentrated in the pyramidal neurons of layer V (Shin et al., 2006), the area of focus in the current study. Our findings demonstrate that the number of Nogo-A-positive neurons is decreased, but the number of Nogo-A-positive non-neural cells is increased in layer V of the cortex ipsilateral to the injury, though it was not significantly changed in the cortex contralateral to the injury. In contrast, Marklund and associates (2006) found that Nogo-A is significantly increased in both cortical neurons and glia of the injured hemisphere from days 1–7 after FPI, though they did not examine its expression at later time points and or in the contralateral cortex. The differences in our findings compared to those of Marklund and colleagues may be due to the different models of TBI studied, given that Nogo-A expression patterns vary with injury severity in stroke and spinal cord injury models (Cheatwood et al., 2008; Josephson et al., 2001). The increased expression of Nogo-A surrounding the cortical contusion in the current study suggests that an increase in inhibitory molecules may have played a role in the inhibition of markers of plasticity

surrounding the injury. However, it cannot easily explain the limited dendritic regrowth seen in the contralateral cortex, since NogoA expression was not significantly changed there. It remains possible that other inhibitory molecules not examined in the current study such as CSPG play a role.

Synaptophysin immunoreactivity was not significantly changed in the cortex contralateral to CCI, but there was a transient increase in the injured hemisphere seen at day 14 post-CCI. This increase reflected a labeling pattern of dense clusters of immunoreactive puncta, in contrast to the more diffuse distribution typical of intact and contralateral cortex. Because this was a time point of greatly reduced dendritic density in this region, it is possible that this transient increase reflects a stage of compensatory synaptogenesis. However, it may also indicate an abnormal accumulation of this presynaptic vesicle protein, because disrupted transport and abnormal accumulation of synaptophysin occurs during axonal degeneration (Ferrer, 2002; Tesseur et al., 2000). Clarifying this would require an electron microscopic analysis of this area. Previous studies have found decreases in neocortical synapse-related proteins and synaptic structures after TBI, at least early after the injury. Campbell and colleagues found that spine density visualized using Golgi-Cox staining was significantly decreased by 24 h post-injury, but returned to baseline by 1 week following moderate FPI (Campbell et al., 2011). Ansari and colleagues (Ansari et al., 2008b) found that proteins such as PSD-95, synapsin-I, and SAP-97 were decreased in the cortex surrounding the injury between 24 and 96 h post-CCI. Similarly, Ding and colleagues (2009) found reduced synaptophysin in the ipsilateral cortex up to 48 h post-injury in an impact-acceleration model of TBI. None of these studies, however, examined cortex out to 14 days. In contrast to these studies, we did not find a decrease in synaptophysin levels at any time point, but it is quite possible for a transient decrease to be missed, given that the earliest time point examined was 3 days post-injury. However, in the hippocampus, moderate CCI elevates synaptophysin levels at both early (24–72 h) and later (21 days) post-injury time points (Thompson et al., 2006). After FPI, spine density was decreased in the dentate gyrus by 24 h post-FPI, but increased above control levels by 1 week post-injury (Campbell et al., 2011). These findings suggest that TBI-induced changes in synaptic proteins vary considerably with time and region examined, in addition to injury severity.

Conclusion

Our data indicate that unlike what is seen in models of focal stroke, structural cortical plasticity is compromised following focal traumatic brain injury. Some possible reasons for this discrepancy include differences in injury severity, extent of pathological secondary events, and expression of growth inhibitory molecules. These findings have implications for rehabilitation and the promotion of plasticity as potential therapeutic strategies following TBI. Further studies are needed to elucidate the mechanisms of compromised plasticity, as well as to reveal ways to over come it.

Acknowledgments

Support for this work was provided by DePaul University Research Council and College of Liberal Arts and Sciences Undergraduate Grants to D.A.K. We thank Dr. R.P. Allred for help with statistical analyses.

Author Disclosure Statement

No competing financial interests exist.

References

Adkins, D.L., Campos, P., Quach, D., Borromeo, M., Schallert, K., and Jones, T.A. (2006). Epidural cortical stimulation enhances motor function after sensorimotor cortical infarcts in rats. Exp. Neurol. 200, 356–370.

Adkins, D.L., Voorhies, A.C., and Jones, T.A. (2004). Behavioral and neuroplastic effects of focal endothelin-1 induced sensorimotor cortex lesions. Neuroscience 128, 473–486.

Allred, R.P., and Jones, T.A. (2008). Experience—a double edged sword for restorative neural plasticity after brain damage. Future Neurol. 3, 189–198.

Ansari, M.A., Roberts, K.N., and Scheff, S.W. (2008b). A time course of contusion-induced oxidative stress and synaptic proteins in cortex in a rat model of TBI. J. Neurotrauma 25, 513–526.

Ansari, M.A., Roberts, K.N., and Scheff, S.W. (2008a). Oxidative stress and modification of synaptic proteins in hippocampus after traumatic brain injury. Free Radic. Biol. Med. 45, 443–452.

Baddeley, A.J., Gundersen, H.J., and Cruz-Orive, L.M. (1986). Estimation of surface area from vertical sections. J. Microsc. 142, 259–276.

Becerra, G.D., Tatko, C.M., Pak, E.S., Murashov, A.K., and Hoane, M.R. (2007). Transplantation of GABAergic neurons but not astrocytes induces recovery of sensorimotor function in the traumatically injured brain. Behav. Brain Res. 179, 118–125.

Brown, C.E., and Murphy, T.H. (2008). Livin' on the edge: imaging dendritic spine turnover in the peri-infarct zone during ischemic stroke and recovery. Neuroscientist 14, 139–146.

Campbell, J.N., Churn, S.B., and Register, D. (2011). Traumatic brain injury causes an FK506-sensitive loss and an overgrowth of dendritic spines in rat forebrain. J. Neurotrauma.

Carmichael, S.T., and Chesselet, M.F. (2002). Synchronous neuronal activity is a signal for axonal sprouting after cortical lesions in the adult. J. Neurosci. 22, 6062–6070.

Cheatwood, J.L., Emerick, A.J., Schwab, M.E., and Kartje, G.L. (2008). Nogo-A expression after focal ischemic stroke in the adult rat. Stroke 39, 2091–2098.

Chen, M.S., Huber, A.B., Van Der Haar, M.E., Frank, M., Schnell, L., Spillmann, A.A., Christ, F., and Schwab, M.E. (2000). Nogo-A is a myelin-associated neurite outgrowth inhibitor and an antigen for monoclonal antibody IN-1. Nature 403, 434–439.

Chu, C.J., and Jones, T.A. (2000). Experience-dependent structural plasticity in cortex heterotopic to focal sensorimotor cortical damage. Exp. Neurol. 166, 403–414.

Desalles, A.A., Newlon, P.G., Katayama, Y., Dixon, C.E., Becker, D.P., Stonnington, H.H., and Hayes, R.L. (1987). Transient suppression of event-related evoked potentials produced by mild head injury in the cat. J. Neurosurg. 66, 102–108.

Ding, J.Y., Kreipke, C.W., Schafer, P., Schafer, S., Speirs, S.L., and Rafols, J.A. (2009). Synapse loss regulated by matrix metalloproteinases in traumatic brain injury is associated with hypoxia inducible factor-1alpha expression. Brain Res. 1268, 125–134.

Dixon, C.E., Clifton, G.L., and Lighthall, J.W. (1991). A controlled cortical impact model of traumatic brain injury in the rat. J Neurosci. Methods 39, 253–262.

Donoghue, J.P.W., and Wise, S.P. (1982). The motor cortex of the rat: Cytoarchitecture and microstimulation mapping. J. Comp. Neurol. 212, 76–88.

Ferrer, I. (2002). Synaptic pathology and cell death in the cerebellum in Creutzfeldt-Jacob disease. Cerebellum 1, 213–222.

Folkerts, M.M., Berman, R.F., Muizelaar, J.P., and Rafols, J.A. (1998). Disruption of MAP-2 immunostaining in rat hippocampus after traumatic brain injury. J. Neurotrauma 15, 349–363.

Funahashi, S., Hasegawa, T., Nagano, A., and Sato, K. (2008). Differential expression patterns of messenger RNAs encoding Nogo receptors and their ligands in the rat central nervous system. J. Comp. Neurol. 506, 141–160.

Grandpre, T., Nakamura, F., Vartanian, T., and Strittmatter, S.M. (2000). Identification of the Nogo inhibitor of axon regeneration as a Reticulon protein. Nature 403, 439–444.

Gundersen, H.J., and Jensen, E.B. (1987). The efficiency of systematic sampling in stereology and its prediction. J. Microsc. 147, 229–263.

Hall, K.D., and Lifshitz, J. (2010). Diffuse traumatic brain injury initially attenuates and later expands activation of the rat somatosensory whisker circuit concomitant with neuroplastic responses. Brain Res. 1323, 161–173.

Hall, E.D., Bryant, Y.D., Cho, W., and Sullivan, P.G. (2008). Evolution of post-traumatic neurodegeneration after controlled cortical impact traumatic brain injury in mice and rats as assessed by the de Olmos silver and fluorojade staining methods. J. Neurotrauma 25, 235–247.

Harris, N.G., Carmichael, S.T., Hovda, D.A., and Sutton, R.L. (2009). Traumatic brain injury results in disparate regions of chondroitin sulfate proteoglycan expression that are temporally limited. J. Neurosci. Res. 87, 2937–2950.

Hernandez, T.D., and Schallert, T. (1988). Seizures and recovery from experimental brain damage. Exp. Neurol. 102, 318–324.

Hoane, M.R., Pierce, J.L., Holland, M.A., Birky, N.D., Dang, T., Vitek, M.P., and McKenna, S.E. (2007). The novel apolipoprotein E-based peptide COG1410 improves sensorimotor performance and reduces injury magnitude following cortical contusion injury. J. Neurotrauma 24, 1108–1118.

Hovda, D.A. (1996). Metabolic dysfunction, in: *Neurotrauma*. R.K. Narayan, J.E. Wilberger, and J.T. Povlishock, eds. McGraw-Hill: New York, pps. 1459–1478.

Hsu, J.E., and Jones, T.A. (2006). Contralesional neural plasticity and functional changes in the less-affected forelimb after large and small cortical infarcts in rats. Exp. Neurol. 201, 479–494.

Hsu, J.E., and Jones, T.A. (2005). Time-sensitive enhancement of motor learning with the less-affected forelimb after unilateral sensorimotor cortex lesions in rats. Eur. J. Neurosci. 22, 2069–2080.

Huh, J.W., Raghupathi, R., Laurer, H.L., Helfaer, M.A., and Saatman, K.E. (2003). Transient loss of microtubule-associated protein 2 immunoreactivity after moderate brain injury in mice. J. Neurotrauma 20, 975–984.

Ip, E.Y., Zanier, E.R., Moore, A.H., Lee, S.M., and Hovda, D.A. (2003). Metabolic, neurochemical, and histologic responses to vibrissa motor cortex stimulation after traumatic brain injury. J. Cereb. Blood Flow Metab. 23, 900–910.

Jones, T.A., Allred, R.P., Adkins, D.L., Hsu, J.E., O'Bryant, A., and Maldonado, M.A. (2009). Remodeling the brain with behavioral experience after stroke. Stroke 40, S136–S138.

Jones, T.A., and Schallert, T. (1992). Overgrowth and pruning of dendrites in adult rats recovering from neocortical damage. Brain Res. 581, 156–160.

Jones, T.A., and Schallert, T. (1994). Use-dependent growth of pyramidal neurons after neocortical damage. J. Neurosci. 14, 2140–2152.

Jones, T.A., Kleim, J.A., and Greenough, W.T. (1996). Synaptogenesis and dendritic growth in the cortex opposite unilateral sensorimotor cortex damage in adult rats: a quantitative electron microscopic examination. Brain Res. 733, 142–148.

Jones, T.A. (1999). Multiple synapse formation in the motor cortex opposite unilateral sensorimotor cortex lesions in adult rats. J. Comp. Neurol. 414, 57–66.

Jortner, B.S., Dyer, K., Walton, A., and Ehrich, M. (1997). Synaptophysin immunoreactive axonal swelling in p-bromophenylacetylurea-induced neuropathy. Neruotoxicology 18, 161–168.

Josephson, A., Widenfalk, J., Widmer, H.W., Olson, L., and Spenger, C. (2001). NOGO mRNA expression in adult and fetal human and rat nervous tissue and in weight drop injury. Exp. Neurol. 169, 319–328.

Kaas, J.H., Merzenich, M.M., and Killackey, H.P. (1983). The reorganization of somatosensory cortex following peripheral nerve damage in adult and developing mammals. Annu. Rev. Neurosci. 6, 325–356.

Kelly, D.F., Kozlowski, D.A., Haddad, E., Echiverri, A., Hovda, D.A., and Lee, S.M. (2000). Ethanol reduces metabolic uncoupling following experimental head injury. J. Neurotrauma 17, 261–272.

Kleim, J.A., and Jones, T.A. (2008). Principles of experience-dependent neural plasticity: implications for rehabilitation after brain damage. J. Speech Lang. Hear. Res. 51, S225–S239.

Kozlowski, D.A., James, D.C., and Schallert, T. (1996). Use-dependent exaggeration of neuronal injury after unilateral sensorimotor cortex lesions. J. Neurosci. 16, 4776–4786.

Lehr, R.P. (2010). Neuroplasticity and rehabilitation therapy, in: *Traumatic Brain Injury: Rehabilitation, Treatment, and Case Management*. M.J. Ashley, ed. CRC Press: New York, pps. 455–469.

Li, H.H., Lee, S.M., Cai, Y., Sutton, R.L., and Hovda, D.A. (2004). Differential gene expression in hippocampus following experimental brain trauma reveals distinct features of moderate and severe injuries. J. Neurotrauma 21, 1141–1153.

Liu, H., Ng, C.E., and Tang, B.L. (2002). Nogo-A expression in mouse central nervous system neurons. Neurosci. Lett. 328, 257–260.

Luke, L.M., Allred, R.P., and Jones, T.A. (2004). Unilateral ischemic sensorimotor cortical damage induces contralesional synaptogenesis and enhances skilled reaching with the ipsilateral forelimb in adult male rats. Synapse 54, 187–199.

Madow, L.H., and Madow, W.G. (1994). On the theory of systematic sampling. Ann. Math. Statist. 15, 1–24.

Marklund, N., Fulp, C.T., Shimizu, S., Puri, R., McMillan, A., Strittmatter, S.M., and McIntosh, T.K. (2006). Selective temporal and regional alterations of Nogo-A and small proline-rich repeat protein 1A (SPRR1A) but not Nogo-66 receptor (NgR) occur following traumatic brain injury in the rat. Exp. Neurol. 197, 70–83.

Mir, H.M., Tatsukawa, K.J., Carmichael, S.T., Chesselet, M.F., and Kornblum, H.I. (2004). Metabolic correlates of lesion-specific plasticity: an in vivo imaging study. Brain Res. 1002, 28–34.

Monnerie, H., Tang-Schomer, M.D., Iwata, A., Smith, D.H., Kim, H.A., and Le Roux, P.D. (2010). Dendritic alterations after dynamic axonal stretch injury in vitro. Exp. Neurol. 224, 415–423.

Moore, A.H., Osteen, C.L., Chatziioannou, A.F., Hovda, D.A., and Cherry, S.R. (2000). Quantitative assessment of longitudinal metabolic changes in vivo after traumatic brain injury in the adult rat using FDG-microPET. J. Cereb. Blood Flow Metab. 20, 1492–1501.

Nishibe, M., Barbay, S., Guggenmos, D., and Nudo, R.J. (2010). Reorganization of motor cortex after controlled cortical impact in rats and implications for functional recovery. J. Neurotrauma 27, 2221–2232.

Nudo, R.J. (2007). Postinfarct cortical plasticity and behavioral recovery. Stroke 38, 840–845.

Passineau, M.J., Zhao, W., Busto, R., Dietrich, W.D., Alonso, O., Loor, J.Y., Bramlett, H.M., and Ginsberg, M.D. (2000). Chronic metabolic sequelae of traumatic brain injury: prolonged suppression of somatosensory activation. Am. J. Physiol. Heart Circ. Physiol. 279, H924–H931.

Peters, A., Palay, S., and Webster, H.D. (1991). *The Fine Structure of the Nervous System, Neurons and their Supporting Cells*. Oxford University Press: New York.

Phillips, L.L., and Reeves, T.M. (2001). Interactive pathology following traumatic brain injury modifies hippocampal plasticity. Restor. Neurol. Neurosci. 19, 213–235.

Posmantur, R.M., Kampfl, A., Taft, W.C., Bhattacharjee, M., Dixon, C.E., Bao, J., and Hayes, R.L. (1996). Diminished microtubule-associated protein 2 (MAP2) immunoreactivity following cortical impact brain injury. J. Neurotrauma 13, 125–137.

R Development Core Team. (2010). R: A language and environment for statistical computing. R Foundation for Statistical Computing. Vienna, Austria.

Reeves, T.M., Kao, C.Q., Phillips, L.L., Bullock, M.R., and Povlishock, J.T. (2000). Presynaptic excitability changes following traumatic brain injury in the rat. J. Neurosci. Res. 60, 370–379.

Schallert, T., Kozlowski, D.A., Humm, J.L., and Cocke, R.R. (1997). Use-dependent structural events in recovery of function, in: *Brain Plasticity, Advances in Neurology*. H.-J. Freund, B.A. Sabe, and O.W. Witte, eds. Raven Press: New York, p. 73.

Scheff, S.W., Price, D.A., Hicks, R.R., Baldwin, S.A., Robinson, S., and Brackney, C. (2005). Synaptogenesis in the hippocampal CA1 field following traumatic brain injury. J. Neurotrauma 22, 719–732.

Schmued, L.C., and Hopkins, K.J. (2000). Fluoro-Jade B: a high affinity fluorescent marker for the localization of neuronal degeneration. Brain Res. 874, 123–130.

Shin, J.W., Shim, E.S., Hwang, G.H., Jung, H.S., Park, J.H., and Sohn, N.W. (2006). Cell size-dependent Nogo-A expression in layer V pyramidal neurons of the rat primary somatosensory cortex. Neurosci. Lett. 394, 117–120.

Stein, D.G. (2007). Concepts of CNS plasticity and their implications for understanding recovery after brain damage, in: *Brain Injury Medicine: Principles and Practice*. N.D. Zasler, D.I. Katz, and R.D. Zafonte, eds. Demos: New York, pps. 97–108.

Sutton, R.L., Lescaudron, L., and Stein, D.G. (1993). Unilateral cortical contusion injury in the rat: vascular disruption and temporal development of cortical necrosis. J. Neurotrauma 10, 135–149.

Taft, W.C., Yang, K., Dixon, C.E., and Hayes, R.L. (1992). Microtubule-associated protein 2 levels decrease in hippocampus following traumatic brain injury. J. Neurotrauma 9, 281–290.

Tesseur, I., Van Dorpe, J., Bruynseels, K., Bronfman, F., Sciot, R., Vanlommel, A., and Vanleuvan, F. (2000). Prominent axonopathy and disruption of axonal transport in transgenic mice expressing human apolipoprotein E4 in neurons of brain and spinal cord. Am. J. Pathol. 157, 495–510.

Thompson, S.N., Gibson, T.R., Thompson, B.M., Deng, Y., and Hall, E.D. (2006). Relationship of calpain-mediated proteolysis to the expression of axonal and synaptic plasticity markers following traumatic brain injury in mice. Exp. Neurol. 201, 253–265.

Voorhies, A.C., and Jones, T.A. (2002). The behavioral and dendritic growth effects of focal sensorimotor cortical damage depend on the method of lesion induction. Behav. Brain Res. 133, 237–246.

Wiley, J.L., Compton, A.D., Pike, B.R., Temple, M.D., McElderry, J.W., and Hamm, R.J. (1996). Reduced sensorimotor reactivity following traumatic brain injury in rats. Brain Res. 716, 47–52.

Wise, S.P., and Donoghue, J.P. (1986). Motor cortex of rodents, in: *Cerebral Cortex*. E.G. Jones and A. Peters, eds. Plenum: New York, pps. 243–270.

Zorner, B., and Schwab, M.E. (2010). Anti-Nogo on the go: from animal models to a clinical trial. Ann. NY Acad. Sci. 1198(Suppl. 1), E22–E34.

Address correspondence to:
Dorothy A. Kozlowski, Ph.D.
DePaul University
Department of Biological Sciences
2325 North Clifton
Chicago, IL 60614

E-mail: dkozlows@depaul.edu